Journal of Materials Chemistry C

PAPER

View Article Online
View Journal | View Issue

Cite this: J. Mater. Chem. C, 2017, 5, 12249

Stable monolayer α-phase of CdTe: strain-dependent properties†

E. Unsal, *[a] R. T. Senger [ab] and H. Sahin [bc]

Received 11th September 2017,
Accepted 1st November 2017

DOI: 10.1039/c7tc04151a

rsc.li/materials-c

CdTe is a well known and widely used binary compound for optoelectronic applications. In this study, we propose the thinnest, free standing monolayer of CdTe which has a tetragonal-PbO (α-PbO) symmetry. The structural, electronic, vibrational and strain dependent properties are investigated by means of first principles calculations based on density functional theory. Our results demonstrate that monolayer α-CdTe is a dynamically stable and mechanically flexible material. It is found that the thinnest monolayer crystal of CdTe is a semiconductor with a direct band gap of 1.95 eV, which corresponds to red light in the visible spectrum. Moreover, it is found that the band gap can be tunable under biaxial strain. With its strain-controllable direct band gap within the visible spectrum, the stable α-phase of monolayer CdTe is a suitable candidate for optoelectronic device applications.

I. Introduction

Since technology proceeds towards the nanoscale, the synthesis of low-dimensional materials has become an important issue. Graphene, a one-atom-thick crystal of C-atoms arranged in a honeycomb structure, was successfully synthesized in 2004.[1] Although graphene possesses extraordinary physical properties,[2,3] having a zero band gap in its electronic structure restricts its application in nanotechnology.[4] Over the last decade, graphene has triggered the search for novel two-dimensional (2D) materials in various categories such as transition metal dichalcogenides[5–7] (*e.g.* MoS_2[8–12] and WS_2[13,14]) and II–VI binary compounds (*e.g.* CdSe[15] and ZnSe[16,17]). The II–VI group semiconductors are well-known materials and there have been a wide range of theoretical and experimental studies on these materials.[18–22]

As a II–VI binary compound, bulk CdTe has been widely studied in the last half-century.[23–27] Bulk CdTe has a direct band gap of approximately 1.50 eV, which optimally matches with the solar spectrum.[28] Therefore, this material has extensive usage in optoelectronic device applications such as photo-detectors and infrared and gamma-ray detectors.[29–33] Beyond its bulk form, dimensionally reduced CdTe structures, *e.g.* quantum dots and rods,[34] have attracted great attention due to their composition- and size-dependent absorption and emission spectrum.[35,36] Gupta *et al.* succeeded in reducing the thickness of a CdTe film in a CdS/CdTe solar cell, which is the thinnest CdTe cell with high efficiency.[39] Moreover, Sun *et al.* stated that they could improve quantum-dot-based light emitting diodes (LEDs) with enhanced electroluminescence efficiency and lifetimes for long-term operations. Considering their findings, they also reported that quantum-dot-based LEDs would be used in the manufacture of flat-panel displays (such as televisions and monitors).[37] Recently, Ithurria *et al.* have reported the synthesis of cadmium chalcogenide (CdSe, CdS and CdTe) nanoplatelets with various thicknesses.[40] They showed that these classes of colloidal semiconductor materials exhibit physical and optical properties such as tunable thickness, controllable lateral dimension and enhanced oscillator strength, which make the colloidal platelets suitable for nonlinear optical devices.[38] In spite of intensive studies on low dimensional CdTe, the monolayer phase of CdTe has never been investigated before.

Herein, we investigate the structural, electronic and mechanical properties of a phase of monolayer CdTe by employing first principles calculations based on DFT. Monolayer CdTe is found to be dynamically stable and has two prominent Raman-active modes. Monolayer CdTe is a direct gap semiconductor with its strain-tunable band gap energy and has a low in-plane stiffness.

The paper is organized as follows: in Section II information about our computational methodology is given. Then, the possible structural phases of monolayer CdTe are discussed in Section III. Identification of the structural phase of monolayer α-CdTe is presented in Section IV. In Section V the vibrational properties are presented. The electronic properties of the structure are discussed in Section VI and the strain dependent properties are discussed in Section VII. The final section, Section VIII, is allocated for the conclusion of our study.

[a] Department of Physics, Izmir Institute of Technology, 35430, Izmir, Turkey. E-mail: elifunsal@iyte.edu.tr
[b] ICTP-ECAR Eurasian Center for Advanced Research, Izmir Institute of Technology, 35430, Izmir, Turkey
[c] Department of Photonics, Izmir Institute of Technology, 35430, Izmir, Turkey

† PACS numbers: 71.15.Mb, 73.61.Ga, 81.40.Jj.

II. Computational methodology

All calculations were performed using DFT and projector-augmented wave (PAW) potentials as implemented in the Vienna *ab initio* simulation package (VASP).[41–43] The Perdew–Burke–Ernzerhof (PBE) form of the generalized gradient approximation (GGA)[44] was used for the description of electron exchange and correlation. The Heyd–Scuseria–Ernzerhof (HSE06) hybrid functional was included on top of GGA for band gap estimation.[45] The van der Waals forces were included using the DFT-D2 method of Grimme.[46,47] The Bader technique was adopted in order to determine the charge transfer in the structure.[48,49]

The structure was relaxed until the total energy difference between consecutive electronic steps reached the level of 10^{-5} eV and Hellmann–Feynman forces on each unit cell were less than 10^{-4} eV Å^{-1}. Gaussian smearing was used with a broadening of 0.05 eV and the pressure on the unit cell was reduced to a value less than 1.0 kB in all three directions. To avoid interactions between adjacent monolayers, a vacuum space of 12 Å was included. For the Brillouin Zone (BZ) integration, a 16 × 16 × 1 Γ-centered mesh was used for the primitive unit cell.

Moreover, the vibrational properties of monolayer α-CdTe were investigated for a 6 × 6 × 1 supercell with 144 atoms using the small displacement method as implemented in the PHON code.[50] For calculating the cohesive energy per atom, E_{Cohesive}, we used the following formula:

$$E_{\mathrm{Cohesive}} = \frac{1}{n_{\mathrm{tot}}}[n_{\mathrm{Cd}}E_{\mathrm{Cd}} + n_{\mathrm{Te}}E_{\mathrm{Te}} - E_{\mathrm{ML}}], \quad (1)$$

where E_{Cd} and E_{Te} represent the energies of single isolated Cd and Te atoms. E_{ML} stands for the total energy of monolayer α-CdTe and n_{tot}, n_{Cd} and n_{Te} denote the total number of atoms, the number of Cd atoms and the number of Te atoms within the unit cell, respectively. The calculated values of cohesive energies are discussed in Section III.

For the calculation of the elastic constants of the α-phase, a 4 × 4 × 1 64-atom supercell was considered. Strains were applied along the *x*- and *y*-axis by changing the lattice parameters along each direction. We applied uniaxial strains, ε_x and ε_y, and a biaxial strain along both directions. Strain energy E_{S} was calculated by subtracting the ground state energy of the system from the energy of the system under applied load. Using quadratic regression, calculated data were fitted to the following equation:

$$E_{\mathrm{S}} = c_1\varepsilon_x^{\,2} + c_2\varepsilon_y^{\,2} + c_3\varepsilon_x\varepsilon_y \quad (2)$$

and the coefficients of c_i were obtained. In-plane stiffness along the *x*- and *y*-axis is calculated using the following formulas:[51]

$$C_x = \frac{1}{A_0}\left(2c_1 - \frac{c_3^{\,2}}{2c_2}\right) \quad (3)$$

$$C_y = \frac{1}{A_0}\left(2c_2 - \frac{c_3^{\,2}}{2c_1}\right) \quad (4)$$

where A_0 is the unit cell area of the unstrained system and c_1, c_2 and c_3 are constants obtained using eqn (2). For the calculation of Poisson's ratio, we used the formulas, $\nu_x = c_3/2c_1$ and $\nu_y = c_3/2c_2$, where ν_x and ν_y are the ratios in the *x* and *y* directions.[51] The calculated values of the elastic constants are discussed in Section VII.

III. Structural phases of monolayer CdTe

In this section, we investigate two-dimensional phases of CdTe, which include planar hexagonal (graphene-like), buckled hexagonal (silicene-like), 1T and 1H phases. As square lattices, black phosphorus (bp-CdTe) and α-CdTe structural phases are also studied. In order to find the energetically most favorable phase of monolayer CdTe, we calculate the cohesive energy of each phase and compare it with those of the other phases. We also perform the phonon calculation through the whole BZ for each phase to analyze their dynamic stability. It is found that the cohesive energies for the 1H, planar and buckled hexagonal phases are 2.05 eV atom^{-1}, 1.90 and 1.92 eV atom^{-1}, respectively. As seen in Fig. 3, the planar hexagonal structure is energetically the least favorable phase among all of these structures and the phonon-band diagram of the planer phase reveals its dynamic instability. The cohesive energies of monolayer bp-CdTe, 1T and α-CdTe phases are calculated to be 2.13, 2.14 and 2.15 eV atom^{-1}, respectively. Although these energy values are very close to each other, it is seen that 1T and bp-CdTe phases are dynamically unstable. As seen in Fig. 1, all of the hexagonal structures as well as bp-CdTe have negative frequencies.

Among these monolayer phases of CdTe, the α-phase is energetically the most favorable structure, which indicates that monolayer CdTe is more likely to have the α-phase in comparison to other possible structural phases. In addition, the α-phase is found to be dynamically stable. Therefore, in the following sections, the characteristic properties of monolayer α-CdTe are presented in detail.

IV. Structural properties of α-CdTe

As a well-known semiconducting material, CdTe crystallizes in the zinc-blende (zb-) structure under ambient conditions of temperature and pressure in its bulk form. By varying the pressure, there can occur structural phase transition and it is possible to observe rocksalt, cinnabar or orthorhombic phases of bulk CdTe.[55] Here, we investigate α-PbO-type monolayer CdTe, in which a planar layer of the square Cd lattice is bonded to Te atoms tetrahedrally as seen in Fig. 1. These types of structures belong to the space group *P*4/*nmm*.[56–58] The primitive cell is square and includes two Cd and two Te atoms. As seen in Table 1, the lattice parameter of monolayer α-CdTe is calculated to be 4.66 Å, which is smaller than that of bulk zb-CdTe, and the thickness (vertical distance between the uppermost and the lowermost Te atoms) is found to be 3.55 Å. All the Cd–Te bonds in the monolayer are found to be equal with a value of 2.93 Å, larger than that of the zb-bulk; thus, it is expected that the Cd–Te bonds in the bulk structure are significantly stronger. The Bader charge analysis reveals that each Cd atom donates 0.5*e* to each Te atom which indicates a polar-covalent type bond.

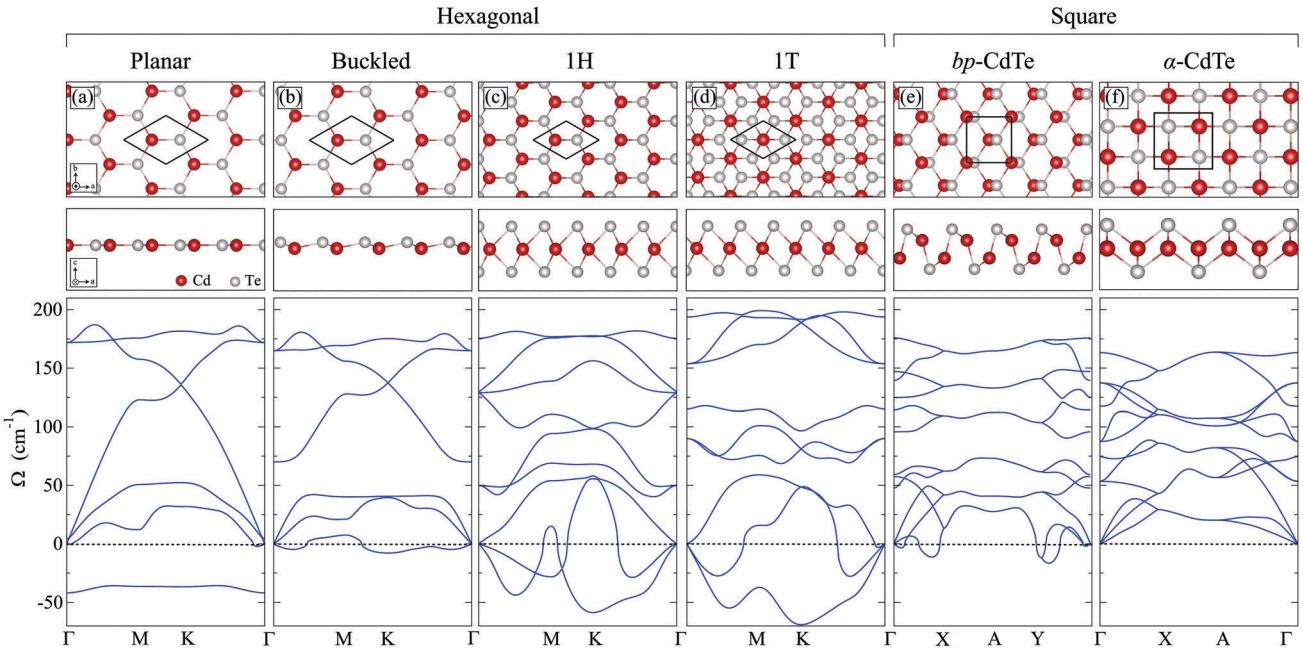

Fig. 1 Top and side views of various monolayer CdTe phases and their phonon band diagrams.

Moreover, we calculate the cohesive energies of the monolayer and the zb-bulk structure in order to understand the formation of the monolayer structure. The cohesive energy is found to be 2.15 and 2.32 eV per atom for the monolayer and bulk zb-CdTe, respectively. Ward *et al.*[52] reported that different phases of CdTe can exist with various cohesive energies in the range between ~1.75 and 2.20 eV per atom. However, the obtained cohesive energy values vary depending on the used DFT methodology.[53,54]

V. Phonons: dynamic stability

In order to investigate the vibrational properties of monolayer α-CdTe, the atoms are slightly distorted from their equilibrium positions. It is found that the α-CdTe crystal can generate the required restoring force and remain dynamically stable. As is seen in Fig. 1(f), the vibrations occur at low frequencies smaller than 200 cm^{-1}, which indicates soft phonon modes, *i.e.* the flexibility of the structure. Since Cd and Te atoms are relatively large atoms, the Cd–Te bond length in the crystal is large which means that α-CdTe has a flexible nature.

The phonon spectrum of monolayer α-CdTe includes 12 phonon branches. 3 of which are acoustic (longitudinal acoustic (LA), transverse acoustic (TA) and out-of-plane flexural (ZA)), and 9 of them are optical vibrational modes. 6 of the optical vibrational modes are demonstrated in Fig. 2 due to the degeneracy in three of them. The optical vibrational mode with the highest frequency, which is found to be 163.7 cm^{-1}, corresponds to an out-of-plane mode in which both of the Te sub-layers move opposite to the Cd sub-layer. Moreover, there are three doubly degenerate modes at 53.0, 86.9 and 136.7 cm^{-1}. The characteristics of the modes are in-plane, and at all frequencies, Cd atoms move opposite to each other. In the phonon branches at 53.0 and 136.7 cm^{-1}, the top and the bottom Te sub-layers move in opposite directions; however, both of the Te sub-layers move in the same direction at 86.9 cm^{-1}.

Moreover, Raman intensity calculations are performed for monolayer α-CdTe and it is found that the structure has two prominent Raman-active modes with frequencies of 117.4 and 75.3 cm^{-1}. Both of the Raman-active modes are singly degenerate and have characteristics of out-of-plane counter-phase motion. At a frequency of 75.3 cm^{-1}, Te atoms remain stationary, while Cd atoms move in opposite directions with respect to each other. At a frequency of 117.4 cm^{-1}, Cd atoms are immobile and Te sub-layers move in opposite directions with respect to each other. The Raman activity of these two modes is expected due to the in-plane inversion symmetry of their motions.

Table 1 Calculated parameters for monolayer α-CdTe are the lattice constant, a; the atomic distance between Cd and Te atoms, d_{Cd-Te}; the charge donation of Cd, $\Delta\rho$; the cohesive energy per atom, $E_{Cohesive}$. E_g^{PBE}, $E_g^{PBE+SOC}$ and $E_g^{PBE+SOC+HSE06}$ are the energy gap values calculated with PBE, PBE + SOC and PBE + SOC using the HSE06 method, respectively. Φ and μ present work function and magnetization, respectively. For the calculations of zb-bulk, a conventional cubic cell which consists of eight atoms is considered and work function values are taken from ref. 65

	a (Å)	d_{Cd-Te} (Å)	$\Delta\rho$ (e^-)	$E_{Cohesive}$ (eV per atom)	E_g^{PBE} (eV)	$E_g^{PBE+SOC}$ (eV)	$E_g^{PBE+SOC+HSE06}$ (eV)	Φ (eV)	μ (μ_B)
Monolayer	4.66	2.93	0.5	2.15	1.28	1.02	1.95	5.20	0
zb-Bulk	6.52	2.82	0.5	2.32	0.72	0.45	1.25	5.40–5.65	0

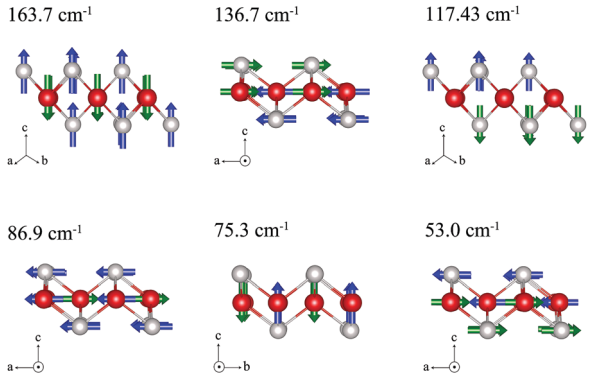

Fig. 2 Phonon modes at the Γ point for monolayer α-CdTe. Red and grey atoms represent the Cd and Te atoms, respectively.

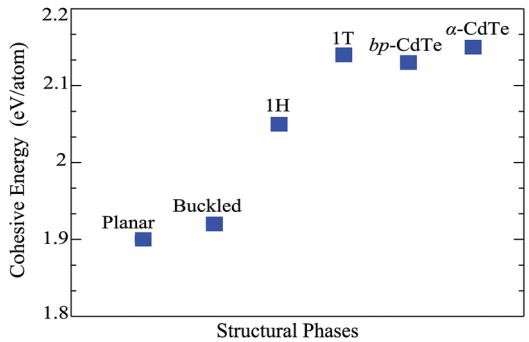

Fig. 3 Calculated cohesive energy values of possible phases of monolayer CdTe are demonstrated. α-CdTe is energetically the most favorable structure among these phases.

In addition, the structures, found to be individually stable, become stable on substrates as well. We search for suitable surfaces on which monolayer α-CdTe can grow. Thus, substrates of α-FeSe with the same structural symmetry as α-CdTe were first investigated. For instance, α-FeSe thin films, belonging to the *P4/nmm* space group as α-CdTe, can be grown on the (001) surface of GaAs substrates using a low-pressure metal organic vapor deposition technique.[59] More recently, it has been observed that single-layer α-FeSe films can grow on $SrTiO_3$ perovskite.[60] As members of the cubic perovskite group, $RbCaF_3$, $CsCaF_3$ and $CsIO_3$ have lattice constants of 4.45 Å, 4.52 Å and 4.67 Å,[61] respectively. Since $CsIO_3$ has a lattice constant very close to that of α-CdTe, it can be an ideal substrate for the growth of the CdTe monolayer.

VI. Electronic properties of α-CdTe

zb-CdTe is a well-known direct band gap semiconductor with a band gap ranging from 1.37 to 1.54 eV.[62] In this section, we examine the electronic structure of monolayer α-CdTe and compare its properties with those of the zb-structure.

Firstly, the band diagram of monolayer α-CdTe is calculated using the PBE functional and an energy gap value of 1.28 eV is found as seen in Table 1. Our calculations reveal that it has a direct band gap at the Γ symmetry point. Inclusion of spin–orbit coupling (SOC) leads to splitting of 0.28 eV at the Γ point and a decrease in the energy gap values as seen in Fig. 4(a). In order to obtain accurate band gap values, the HSE06 method is included on top of SOC and the results show that the band gap values of both structures are increased as seen in Table 1. It is found that zb-bulk and the monolayer α-CdTe structures have energy gap values of 1.25 eV and 1.95 eV, respectively.

Moreover, for valence band maximum (VBM) and conduction band minimum (CBM), 2D-contour plots are drawn for the SOC-added calculations by taking the first BZ as a limit. As seen in Fig. 4(e), adjacent colors indicate the changes in energy of 0.2 eV and the energy values for the VBM at the Γ, X and A

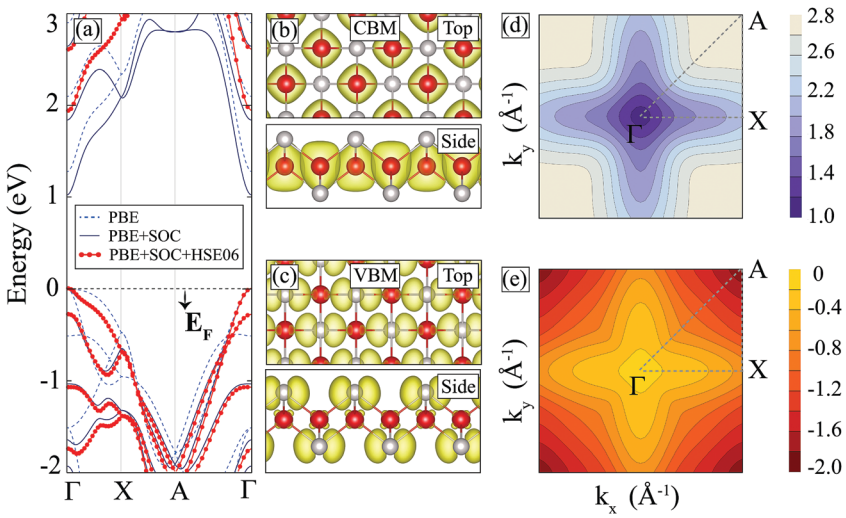

Fig. 4 (a) The energy-band structure of monolayer α-CdTe. Charge densities of (b) CBM and (c) VBM are demonstrated. 2D-contour plots of (d) CBM and (e) VBM are drawn using data obtained from PBE + SOC calculations. The dashed lines represent the irreducible BZ. The color scale demonstrates the energy values in units of eV and the Fermi level (E_F) is set to zero.

points are 0, −0.6 and −2.0 eV, respectively. In addition, the VBM and the CBM are visualized in 3D as seen in Fig. 4(d).

We also investigate the characteristics of the VBM and the CBM and calculate the band decomposed charge densities for monolayer α-CdTe. The results indicate that the VBM mostly possesses the p_x- and p_y-orbitals of the Te atoms; however, there is a small contribution of the d_{yz}- and d_{xz}-orbitals of the Cd atoms. The CBM is dominated by the s-orbitals of the Cd atoms.

Effective mass, a unique feature of the material, is inversely proportional to conductivity. In order to analyze the conduction properties of α-CdTe, the effective mass of electrons and holes is calculated. In the directions of $\Gamma \rightarrow X$ and $\Gamma \rightarrow A$, the effective mass of holes slightly differs from each other and has values of 0.22 and 0.23, respectively. When approaching Γ from X, the effective mass of electrons is nearly the same as the ones located around $\Gamma \rightarrow A$ ($\Gamma \rightarrow X$ 0.46, $\Gamma \rightarrow A$ 0.48).

Work function, a fundamental property of the material, is associated with the ionization energies of atoms in the material. In order to understand the surface properties, the work function of the α-phase is calculated and it is found to be 5.20 eV, which is comparably close to that of MoS_2 (5.88 eV).[63] In addition, it is found that the α-phase can be a suitable candidate for solar photocatalyst chemistry since it possesses suitable band edge positions for water-splitting reactions, where the reduction and oxidation potentials[64] at pH = 7 are −4.03 and −5.26 eV, respectively.

VII. Strain dependent properties of α-CdTe

The applied strain can cause an indirect-to-direct band-gap transition and/or a change in the band gap value.[66,67] In this section, we focus on the strain dependent properties of monolayer α-CdTe and investigate how its mechanical and electronic properties vary with the applied strain.

Firstly, we apply ±1.5% strain with a step size of 0.005 and investigate the structural change. It is found that the Cd–Te bond increases 1% with tensile strain and decreases 1% with compressive strain. This results from the distortion of the charge density with the applied strain. Moreover, our results show that the thickness of monolayer α-CdTe decreases monotonically from compressive to tensile strain for minimizing the influence of the applied strain.

It is calculated that the α-phase has an isotropic in-plane stiffness of 25 N m^{-1}. It appears that compared to the stiffness of monolayer MoS_2 (122 N m^{-1})[63] and graphene (340 N m^{-1}),[68] α-CdTe is a quite flexible and soft material. Moreover, Poisson's ratio, which gives the information about perpendicular enlargement in the crystal structure when it is stretched in a certain direction, is determined by means of DFT calculations. The Poisson's ratio values of monolayer α-CdTe, MoS_2 and graphene are 0.28, 0.26[63] and 0.19,[63] respectively. As is noticed, under applied strain, monolayer MoS_2 and α-CdTe have the same sensitivity and they are more flexible than graphene.

Furthermore, in order to illustrate trends in the band gap for strained α-CdTe (see Fig. 5(a)), we apply biaxial strain in a range where the strains are considered to be between ±10%. In each step, lattice parameters were changed by ±2%. During the stretching and shrinking procedure, the structure remains as a direct gap semiconductor and the constituent orbitals of the VBM remain unchanged. Between the −4% and 10% strain range, Cd-s orbital electrons dominate the conduction band edge (see Fig. 5(c) and (d)). As the structure enlarges, the distance between the s-states opens and the interaction between these states weakens; therefore, the band gap decreases monotonically as seen in Fig. 5(b). As the structure is compressed by more than −4%, band ordering of the conduction band in energy space changes and the conduction band edge is mostly dominated by Te-p_z orbital electrons. Compressing the structure opens the p_z-orbitals which results in a decrease in the band gap value.

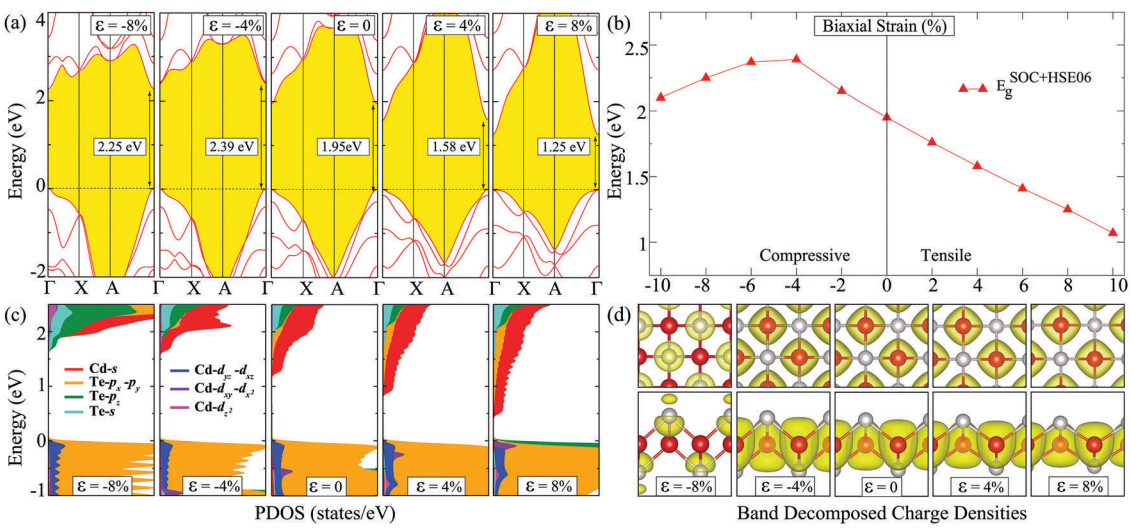

Fig. 5 (a) The electronic band diagrams of monolayer α-CdTe calculated *via* the SOC-added HSE06 method under compressive and tensile strain. The Fermi level is set to zero. (b) The change in the band gap value with applied biaxial strain. (c) Partial density of states and (d) band decomposed charge densities of monolayer α-CdTe under biaxial strain.

Our results reveal that the band gap of the α-CdTe monolayer can be tunable upon biaxial strain.

VIII. Conclusion

In this study, we proposed the thinnest monolayer of CdTe. Structural and vibrational analyses revealed that the structure has the same geometry as α-PbO and it is found that the structure is dynamically stable. Moreover, we performed Raman-intensity calculations and it was found that monolayer α-CdTe has two Raman-active modes with frequencies. In addition, we also examined its electronic structure by including the spin–orbit interaction using the HSE06 method. We found that the structure is a direct band gap semiconductor with a gap value of 1.95 eV which falls in the visible range. Moreover, the strain-dependent electronic properties of monolayer α-CdTe were also studied by applying both compressive and tensile strain. The results showed that the band gap of monolayer α-CdTe alters under biaxial strain. Due to the strain tunable moderate direct band gap, monolayer α-CdTe is a promising material for nanoscale optoelectronic applications.

Conflicts of interest

There are no conflicts to declare.

Acknowledgements

Computational resources for this study were provided by TUBITAK ULAKBIM, High Performance and Grid Computing Center (TR-Grid e-Infrastructure). H. S. acknowledges financial support from TUBITAK under project number 116C073. H. S. also acknowledges support from Bilim Akademisi—The Science Academy, Turkey, under the BAGEP program.

References

1 K. S. Novoselov, A. K. Geim, S. V. Morozov, D. Jiang, Y. Zhang, S. V. Dubonos, I. V. Grigorieva and A. A. Firsov, *Science*, 2004, **306**, 666–669.
2 K. S. Novoselov, A. K. Geim, S. V. Morozov, D. Jiang, M. I. Katsnelson, I. V. Grigorieva, S. V. Dubonos and A. A. Firsov, *Nature*, 2005, **438**, 197–200.
3 A. K. Geim, *Science*, 2009, **324**, 1530–1534.
4 S. J. Zhang, S. S. Lin, X. Q. Li, X. Y. Liu, H. A. Wu, W. L. Xu, P. Wang, Z. Q. Wu, H. K. Zhong and Z. J. Xuab, *Nanoscale*, 2016, **8**, 226–232.
5 H. Fang, S. Chuang, T. C. Chang, K. Takei, T. Takahashi and A. Javey, *Nano Lett.*, 2012, **12**, 3788–3792.
6 M. N. Ali, J. Xiong, S. Flynn, J. Tao, Q. D. Gibson, L. MSchoop, T. Liang, N. Haldolaarachchige, M. HirschbergerN., P. Ong and R. J. Cava, *Nature*, 2014, **514**, 205–208.
7 D. H. Keum, S. Cho, J. H. Kim, D.-H. Choe, H.-J. Sun, M. Kan, H. Kang, J.-Y. Hwang, S. W. Kim, H. Yang, K. J. Chang and Y. H. Lee, *Nat. Phys.*, 2015, **11**, 482–486.
8 K. F. Mak, C. Lee, J. Hone, J. Shan and T. F. Heinz, *Phys. Rev. Lett.*, 2010, **105**, 136805.
9 D. Kong, H. Wang, J. J. Cha, M. Pasta, K. J. Koski, J. Yao and Y. Cui, *Nano Lett.*, 2013, **13**, 1341–1347.
10 B. Radisavljevic, A. Radenovic, J. Brivio and V. Giacomett, *Nat. Nanotechnol.*, 2011, **6**, 147–150.
11 J. Kang, H. Sahin and F. M. Peeters, *Phys. Chem. Chem. Phys.*, 2015, **17**(41), 27742–27749.
12 D. N. Esfahani, O. Leenaerts, H. Sahin, B. Partoens and F. M. Peeters, *J. Phys. Chem. C*, 2015, **119**(19), 10602–10609.
13 B. Mahler, V. Hoepfner, K. Liao and G. A. Ozin, *J. Am. Chem. Soc.*, 2014, **136**, 14121–14127.
14 A. L. Elías, N. Perea-López, A. Castro-Beltrán, A. Berkdemir, R. Lv, S. Feng, A. D. Long, T. Hayashi, Y. A. Kim, M. Endo, H. R. Gutierrez, N. R. Pradhan, L. Balicas, T. E. Mallouk, F. Lopez-Urias, H. Terrones and M. Terrones, *ACS Nano*, 2013, **7**, 5235–5242.
15 J. S. Son, X.-D. Wen, J. Joo, J. Chae, S.-I. Baek, K. Park, H. Kim, K. An, J. H. Yu, S. G. Kwon, S. H. Choi, Z. Wang, Y. W. Kim, Y. Kuk, R. Hoffmann and T. Hyeon, *Angew. Chem., Int. Ed.*, 2009, **48**, 6861–6996.
16 Y. Sun, Z. Sun, S. Gao, H. Cheng, Q. Liu, J. Piao, T. Yao, C. Wu, S. Hu, S. Wei and Y. Xie, *Nat. Commun.*, 2012, **3**, 1057.
17 H. Park, H. Chung and W. Kim, *Mater. Lett.*, 2013, **99**, 172–175.
18 M. A. Hines and P. Guyot-Sionnest, *J. Phys. Chem.*, 1996, **100**, 468–471.
19 L. Manna, D. J. Milliron, A. Meisel, E. C. Scher and A. P. Alivisatos, *Nat. Mater.*, 2003, **2**, 382–385.
20 J. J. Li, Y. A. Wang, W. Z. Guo, J. C. Keay, T. D. Mishima, M. B. Johnson and X. G. Peng, *J. Am. Chem. Soc.*, 2003, **125**, 12567–12575.
21 L. H. Qu, Z. A. Peng and X. G. Peng, *Nano Lett.*, 2001, **1**, 333–337.
22 M.-Z. Huang and W. Y. Ching, *Phys. Rev. B: Condens. Matter Mater. Phys.*, 1993, **47**, 9449–9463.
23 C. B. Murray, D. J. Noms and M. G. Bawendi, *J. Am. Chem. Soc.*, 1993, **115**, 8706–8715.
24 D. Vogel, P. Krüger and J. Pollmann, *Phys. Rev. B: Condens. Matter Mater. Phys.*, 1996, **54**, 5495–5511.
25 O. Zakharov, A. Rubio, X. Blase, M. L. Cohen and S. G. Louie, *Phys. Rev. B: Condens. Matter Mater. Phys.*, 1994, **50**, 10780–10787.
26 L. Ley, R. A. Pollak, F. R. Mcfeely, S. P. Kowalczy and D. A. Shirley, *Phys. Rev. B: Solid State*, 1974, **9**, 600–621.
27 J. R. Chelikowsky and M. L. Cohen, *Phys. Rev. B: Solid State*, 1976, **14**, 556.
28 X. Wu, *Sol. Energy*, 2004, **77**, 803–814.
29 D. Pennicard, B. Pirard, O. Tolbanov and K. Iniewski, *MRS Bull.*, 2017, **42**, 445–450.
30 A. Kanevce, M. O. Reese, T. M. Barnes, S. A. Jensen and W. K. Metzger, *J. Appl. Phys.*, 2017, **121**, 214506.
31 A. Gupta and A. D. Compaan, *Appl. Phys. Lett.*, 2004, **85**, 684.
32 A. Rogalski, *Superlattice detectors*, CRC Press, 2011.
33 K. Hibino, T. Kashiwagi, S. Okuno, K. Yajima, Y. Uchihori, K. Kitamura, T. Takashima, M. Yokota and K. Yoshida, *Astrophys. Space Sci.*, 2007, **309**, 541–544.

34 Z. Adam Peng and X. Peng, *J. Am. Chem. Soc.*, 2001, **123**, 183–184.
35 A. P. Alivisatos, *Science*, 1996, **271**, 933–937.
36 X. Michalet, F. F. Pinaud, L. A. Bentolila, J. M. Tsay, S. Doose, J. J. Li, G. Sundaresan, A. M. Wu, S. S. Gambhir and S. Weiss, *Science*, 2005, **307**, 538–544.
37 Q. Sun, Y. A. Wang, L. S. Li, D. Wang, T. Zhu, J. Xu, C. Yang and Y. Li, *Nat. Photonics*, 2007, **1**, 717–722.
38 S. Ithurria and B. Dubertret, *J. Am. Chem. Soc.*, 2008, **130**, 1316504.
39 A. Gupta, V. Parikh and A. D. Compaan, *Sol. Energy Mater. Sol. Cells*, 2006, **90**, 2263.
40 S. Ithurria, G. Bousquet and B. Dubertret, *J. Am. Chem. Soc.*, 2011, **133**, 3070–3077.
41 G. Kresse and J. Hafner, *Phys. Rev. B: Condens. Matter Mater. Phys.*, 1993, **47**, 558–561.
42 G. Kresse and J. Furthmüller, *Phys. Rev. B: Condens. Matter Mater. Phys.*, 1996, **54**, 11169–11186.
43 G. Kresse and D. Joubert, *Phys. Rev. B: Condens. Matter Mater. Phys.*, 1999, **59**, 1758–1775.
44 J. P. Perdew, K. Burke and M. Ernzerhof, *Phys. Rev. Lett.*, 1996, **77**, 3865–3868.
45 A. V. Krukau, O. A. Vydrov, A. F. Izmaylov and G. E. Scuseria, *J. Chem. Phys.*, 2006, **125**, 224106.
46 S. J. Grimme, *Comput. Chem.*, 2006, **27**, 1787–1799.
47 T. Bucko, J. Hafner, S. Lebegue and J. G. Angyan, *J. Phys. Chem. A*, 2010, **114**, 11814–11824.
48 G. Henkelman, A. Arnaldsson and H. Jonsson, *Comput. Mater. Sci.*, 2006, **36**, 354–360.
49 R. F. W. Bader, *Atoms in Molecules – A Quantum Theory*, Oxford University Press, *Oxford, UK*, 1990.
50 D. Alfe, *Comput. Phys. Commun.*, 2009, **180**, 2622–2633.
51 M. Topsakal, S. Cahangirov and S. Ciraci, *Appl. Phys. Lett.*, 2010, **96**, 091912.
52 D. K. Ward, X. W. Zhou, B. M. Wong, F. P. Doty and J. A. Zimmerman, *J. Chem. Phys.*, 2011, **134**, 244703.
53 X. W. Zhou, D. K. Ward, F. P. Doty, J. A. Zimmerman, B. M. Wong, J. L. Cruz-Campa, G. N. Nielson, J. J. Chavez, D. Zubia and J. C. McClure, *Prog. Photovoltaics Res. Appl.*, 2015, **23**, 1837–1846.
54 D. K. Ward, X. W. Zhou, B. M. Wong, F. P. Doty and J. A. Zimmerman, *Phys. Rev. B: Condens. Matter Mater. Phys.*, 2012, **86**, 245203.
55 *Lolt-Börnstein – Group III Condensed Matter 41B*, ed. O. Madelung, U. Rössler and M. Schulz, Springer-Verlag, Berlin, 1999.
56 *Lolt-Börnstein – Group III Condensed Matter 43A Part 11*, ed. P. Villars and K. Cenzual, Springer-Verlag, *Berlin/Heidelberg*, 2012.
57 P. Canepa, P. Ugliengo and M. Alfredsson, *J. Phys. Chem. C*, 2012, **116**, 21514–22152.
58 N. Hao and S.-Q. Shen, *Phys. Rev. B: Condens. Matter Mater. Phys.*, 2015, **92**(16), 165104.
59 K. W. Liu, J. Y. Zhang, D. Z. Shen, C. X. Shan, B. H. Li, Y. M. Lu and X. W. Fan, *Appl. Phys. Lett.*, 2007, **90**, 262503.
60 J.-F. Ge, Z.-L. Liu, C. Liu, C.-L. Gao, D. Qian, Q.-K. Xue, Y. Liu and J.-F. Jia, *Nat. Mater.*, 2015, **14**, 285–289.
61 A. S. Verma and V. K. Jindal, *J. Alloys Compd.*, 2009, **485**, 514–518.
62 G. Fonthal, L. Tirado-Mejí, J. I. Marín-Hurtado, H. Ariza-Caldero and J. G. Mendoza-Alvarez, *J. Phys. Chem. Solids*, 2000, **61**, 579–583.
63 M. Yagmurcukardes, R. T. Senger, F. M. Peeters and H. Sahin, *Phys. Rev. B*, 2016, **94**, 245407.
64 D. K. Kanan and E. A. Carter, *J. Phys. Chem. C*, 2012, **116**, 9876–9887.
65 S. Hu, Z. Zhu, W. Lia, L. Feng, L. Wu, J. Zhang and J. Gao, *AIP Adv.*, 2011, **1**, 042152.
66 H. Sahin, S. Tongay, S. Horzum, W. Fan, J. Zhou, J. Li, J. Wu and F. M. Peeters, *Phys. Rev. B: Condens. Matter Mater. Phys.*, 2013, **87**, 165409.
67 P. Lu, X. Wu, W. Guo and X. C. Zeng, *Phys. Chem. Chem. Phys.*, 2012, **14**, 13035–13040.
68 C. Lee, X. Wei, J. W. Kysar and J. Hone, *Science*, 2008, **321**, 385–388.